The Journal of Experimental Biology 211, 2243-2251
Published by The Company of Biologists 2008
doi:10.1242/jeb.016147

The contribution of axial fiber extensibility to the adhesion of viscous capture threads spun by orb-weaving spiders

Brent D. Opell*, Brian J. Markley, Charles D. Hannum and Mary L. Hendricks
Department of Biological Sciences, Virginia Polytechnic Institute and State University, Blacksburg, VA 24061, USA.
*Author for correspondence (e-mail: bopell@vt.edu)

Accepted 28 April 2008

SUMMARY

The viscous capture threads produced by over 4000 species of orb-weaving spiders are formed of regularly spaced aqueous droplets supported by a pair of axial fibers. These threads register increased stickiness when spans of increasing lengths contact a surface, indicating that adhesion is recruited from multiple droplets. This study examined threads produced by five species to test the hypothesis that axial fiber extensibility is crucial for this summation of adhesion. It did so by comparing the stickiness of unstretched threads with threads that had been elongated to reduce the extensibility of their axial fibers. As stretching these threads also increased the distance between their droplets, we measured the stickiness of stretched threads with contact plates whose widths were increased in proportion to the degree of thread elongation. We then accounted for the actual thread elongation achieved for each individual's threads and for differences in the five species' absolute thread extensibility. The results showed that in four species thread extensibility contributed positively to adhesion. For three species, thread extensibility and droplet volume together explained the mean per droplet adhesion of threads. Models based on these three species show that, as threads were elongated, increasing amounts of potential adhesion were lost to diminished axial fiber extensibility. These models indicate that approximately one-third of an unstretched viscous thread's stickiness accrues from the adhesive recruitment made possible by axial fiber extensibility.

Key words: orb-web, prey capture thread, thread adhesion, viscous thread.

INTRODUCTION

Viscous capture threads are highly evolved adhesive delivery systems found in orb-webs produced by over 4000 spider species (Fig. 1). They make crucial contributions to the operation of these webs by retaining insects, thereby giving spiders more time to locate, run to and subdue prey that their webs have intercepted (Chacón and Eberhard, 1980; Eberhard, 1986; Eberhard, 1989; Eberhard, 1990). Viscous threads are spun from the spigots of two adjacent silk glands (Foelix, 1996). The flagelliform glands produce a pair of supporting axial fibers, and the aggregate glands coat these fibers with a viscous, aqueous solution that quickly forms into droplets (Peters, 1986; Peters, 1995; Vollrath et al., 1990). The glycoprotein granules that coalesce inside each droplet contribute to thread adhesion (Vollrath and Tillinghast, 1991; Tillinghast et al., 1993) and the hydrophilic compounds in the surrounding fluid attract atmospheric moisture to prevent droplets from drying (Townley, 1990; Vollrath et al., 1990; Townly et al., 1991).

Together with the cob- and sheet-web weaving species descended from them, these orb-weaving spiders comprise the Araneoidea clade, which includes 27% of the 40 024 living spider species (Platnick, 2008). The viscous threads produced by members of this clade replaced the cribellar prey capture threads spun by members of their sister clade, the Deinopoidea (Coddington, 1986; Coddington, 1989; Griswold et al., 1998; Garb et al., 2006). Cribellar capture threads are also supported by a pair of axial fibers. However, these fibers are covered by an outer sheath of fine, dry, looped protein fibrils (Peters, 1984; Peters, 1986; Peters, 1992; Eberhard and Pereira, 1993; Opell, 1999) that are drawn from the spigots of an oval spinning plate, termed the cribellum, by a spider's calamistrum, a setal comb on the metatarsus of each of its fourth legs (Eberhard, 1988; Opell, 2001). Rhythmic adductions of the median spinnerets press the fibril sheath around the supporting strands to produce a thread that has a complex, but often regular, surface configuration (Peters, 1986).

Relative to the volume of material invested in a mm of thread, viscous threads achieved an average of 13 times more stickiness than cribellar thread (Opell, 1998). A factor contributing to the efficiency of viscous thread is its ability to recruit adhesion from multiple droplets using what Opell and Hendricks have described as a suspension bridge mechanism (SBM) (Opell and Hendricks, 2007). Together, the extensibility of a thread's axial fibers and the plasticity of its droplets allow it to bow as the thread is pulled away from a contacting surface. This configuration divides the loading force into perpendicular and parallel vectors, the latter being responsible for recruiting adhesion for droplets that lie interior to the edges of a thread's contact with a surface. As the axial fibers of viscous threads are more extensible than those of cribellar threads (Blackledge and Hayashi, 2006), viscous threads appear better equipped to implement the SBM than do cribellar threads. Documentation of this comes from the observation that viscous thread spans of increasing length register increasing stickiness (Opell and Hendricks, 2007) whereas there is no change in the stickiness of cribellar thread spans of increasing length (Hawthorn and Opell, 2003; Opell and Schwend, in press).

The present study examines more precisely the contribution of axial fiber extensibility to viscous thread adhesion as it tests the hypothesis that reducing the extensibility of a thread's axial fibers reduces its expressed stickiness. It does so by examining the viscous

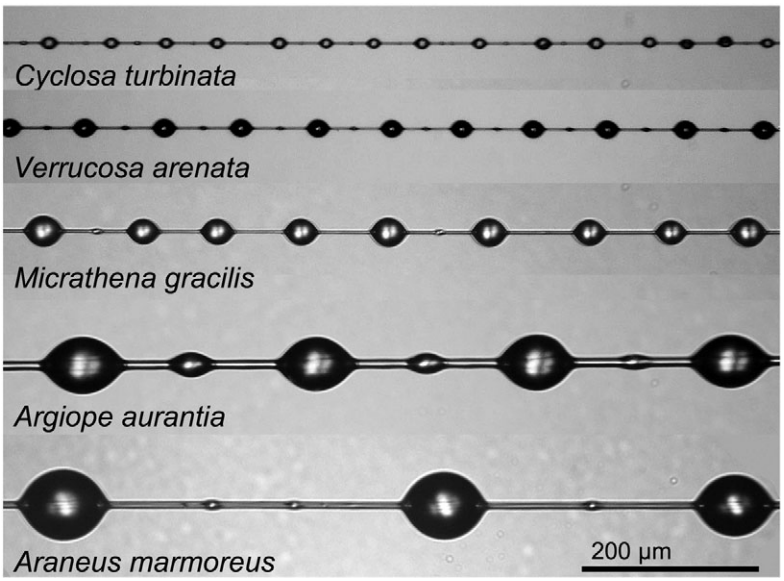

Fig. 1. Capture threads of the five species included in the study, shown at the same magnification.

threads of five araneoid species that have droplet profiles that range from small, closely spaced droplets to large widely spaced droplets (Fig. 1). The stickiness of these threads was first measured under their native tensions and again after they were stretched to two different lengths to reduce the extensibility of their axial fibers. Stretching threads also increases the distance between their droplets (Fig. 2). To maintain the number of droplets that contributed to the stickiness of a thread span, we measured the stickiness of stretched threads with contact plates whose widths were increased in proportion to the degree of thread elongation.

MATERIALS AND METHODS

Species studied and thread collection

We collected web samples from orb-webs constructed by adult females of five species of the family Araneidae [*Araneus marmoreus* Clerck, *Argiope aurantia* Lucas, *Micrathena gracilis* (Walckenaer), *Verrucosa arenata* (Walckenaer) and *Cyclosa turbinata* (Walckenaer)] from sites near Blacksburg, Montgomery Co., VA, USA. Orb-web sectors were collected in the morning, a few hours after webs were spun, using 18 cm-diameter aluminum rings with a 5 mm wide bar across their centers. Double-sided tape on the rim and center bar of each ring held the threads securely. We photographed and measured the stickiness of threads from each web sample in the laboratory under the same relative humidity and temperature within 6.5 h after web samples were collected.

Altering axial fiber extensibility

We collected unstretched capture threads from web-sampling rings using a microscope slide sampler, made by gluing 4.8 mm square brass supports to microscope slides at 4.8 mm intervals. Double-sided Scotch® tape (Tape 665; 3M Co., St Paul, MN, USA) on these supports held the threads securely and maintained their native tensions. Before collecting thread samples, we placed brass bars with double-sided tape on one surface across the collecting ring's rim and center bar to isolate web regions. This permitted us to collect a thread sample from one region of the sampling ring without disturbing threads in other regions. Next, a set of 4–8 threads (depending on the spacing of a species' capture spirals) was collected between two 5 mm-wide bars that were attached to the jaws of a digital caliper in preparation for thread elongation. Double-sided carbon tape (used for mounting specimens to be examined with a scanning electron microscope) secured threads to bars. To hold these threads even more securely, we applied Kores® mimeograph correction fluid (Ink Technology Corp., Tenafly, NJ, USA) along the length of thread spans that contacted the tape. This red fluid is a fast-drying paint whose principal solvent appears to be ether. It immediately adhered to the double-sided tape and, when dry, formed a thin seal on the tape's surface. We then slowly separated the jaws of the caliper at a speed of approximately 232 µm s^{-1} to elongate threads and then collected stretched threads on a microscope slide thread sampler. Threads were elongated to lengths that corresponded to the widths of the contact plates used to measure thread stickiness (Fig. 2). Unstretched threads were measured with contact plates that were 963 µm wide. One set of threads was stretched 2.215 times their native lengths and measured with 2133 µm-wide contact plates. Another set of threads was stretched 3.345 times their native lengths and measured with 3222 µm-wide contact plates. For simplicity, we refer to these

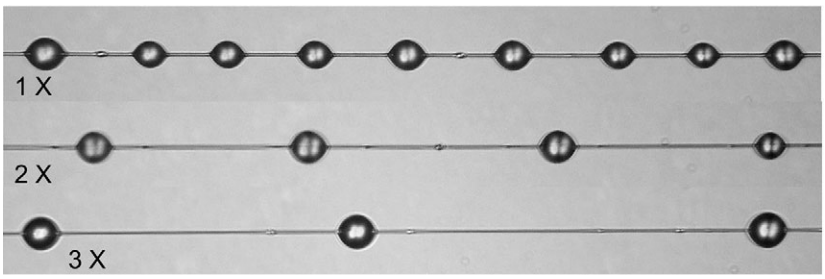

Fig. 2. Capture threads from the web of *M. gracilis* female number 632 at their native (1×) and stretched (2× and 3×) lengths.

elongations as 1×, 2× and 3×. We examined each of these preparations under a dissecting microscope so that we could remove damaged threads, eliminate capture thread spans through which radial threads passed and, in species whose capture threads were very closely spaced, remove threads to achieve spacing appropriate for our stickiness measurement procedures. In the process, we were able to confirm that neither the mimeograph correction fluid or its solvent bled onto the suspended threads, as the spacing and features of the droplets near the edges of these threads were indistinguishable from those at the centers of the threads.

Measuring thread stickiness

As illustrated previously (Opell and Hendricks, 2007), the instrument used to measure thread stickiness allowed us to align a microscope slide sampler so that a thread span was perpendicular to the length of a contact plate. A linear actuator moved thread spans relative to the contact plate, and a sensitive load cell, to which a contact plate was connected by a lever system, recorded the force of adhesion generated as a thread span was pulled from a contact plate. A thread was first pressed against a contact plate at a speed of 0.06 mm s^{-1} until a force of 25 μN was generated and was then immediately withdrawn at the same speed until the thread pulled free of the contact plate. The maximum force registered by a thread was recorded as its stickiness. For each thread elongation, we measured the stickiness of three thread sectors using contact plates of an appropriate width (963, 2133 or 3222 μm) and recorded the mean of these three measurements as a thread's stickiness value for that thread elongation. The contact plates were covered with Scotch Magic® tape (Tape 810; 3M Co.), which provided a smooth acetate surface that maximized thread contact and eliminated the possibility that threads with different droplet profiles might respond differently to a textured surface. This was the same material from the same roll of tape used by Opell and Hendricks to document the operation of the SBM (Opell and Hendricks, 2007). This acetate was replaced frequently and care was taken to ensure that each stickiness measurement was made with an unused sector of a contact plate. Immediately before taking each series of three stickiness measurements, we recorded laboratory temperature, humidity and barometric pressure. All measurements of one individual's threads were completed before measurements of another individual's threads were begun.

Measuring droplet size and spacing

Using techniques described more fully by Opell and Hendricks (Opell and Hendricks, 2007), we photographed the threads of each individual spider at each of the three elongations and measured these digital images with ImageJ (ImageJ, 2006; http://www.uhnresearch.ca/facilities/wcif/imagej/; Bethesda, MD, USA) to characterize the size and spacing of their primary droplets (Table 1). Threads spun by some individuals also have smaller secondary droplets between some of their primary droplets (Fig. 1). As these comprise only a small part of the thread's total volume per mm (*A. aurantia* 1.9%, *A. marmoreus* 3.4%, *M. gracilis* 4.0%, *V. arenata* 0.6%, *C. turbinata* 10.8%; B.D.O. and M.L.H., unpublished observations) and their presence and size were variable, we included only the primary droplets in this study. The profiles of viscous droplets best matched those of a parabola (Opell and Hendricks, 2007). Therefore, we determined droplet volume (DV) using the following formula generated from the formula of a parabola rotated around its *x*-axis (Opell and Hendricks, 2007):

$$DV = (2\,\pi \text{ droplet width}^2 \times \text{droplet length}) / 15.$$

We assessed the range of droplet volumes for an individual spider's threads by first subtracting the mean droplet volume of the thread strand (1×, 2× or 3×) with the smallest mean droplet volume from the thread strand with the greatest mean droplet volume. Next,

Table 1. Features of threads at their native and extended lengths

	A. aurantia (*N*=4)	*A. marmoreus* (*N*=8)	*M. gracilis* (*N*=9)	*V. arenata* (*N*=10)	*C. turbinata* (*N*=8)
Droplet length (μm)					
Unstretched	63.24±4.76	57.67±2.18	29.43±2.20	23.55±2.37	10.73±0.70
2×	62.01±3.40	55.36±3.16	27.28±2.08	25.01±3.12	10.09±0.68
3×	64.46±4.65	60.26±2.70	29.06±2.03	25.98±2.55	10.89±0.53
Droplet width (μm)					
Unstretched	45.39±4.09	43.31±1.67	22.37±1.83	19.18±2.05	8.73±0.63
2×	47.31±3.00	45.42±2.63	21.75±1.61	21.21±2.61	8.59±0.66
3×	49.00±4.13	50.19±2.38	23.52±1.79	21.60±2.10	8.94±0.51
Range of intraindividual droplet volume (%)	31.0±12.0	47.4±5.7	58.5±10.8	57.5±14.3	61.3±12.5
Droplet volume (μm^3)					
Unstretched	58,745±16,383	47,277±5,330	7,132±1,674	4,969±1,902	397±77
2×	60,203±11,575	52,431±9,304	6,236±1,393	6,894±2,545	349±77
3×	67,971±16,516	66,941±9,574	7,716±1,920	6,455±1,836	390±54
Droplets per mm					
Unstretched	3.83±1.36	3.46±0.26	10.98±1.06	10.12±1.24	23.39±7.10
2×	1.69±0.33	1.80±0.13	5.98±0.34	5.38±0.62	11.25±2.16
3×	1.28±0.10	1.24±0.12	4.22±0.31	3.83±0.35	8.83±1.66
Breaking factor	6.33±0.49	6.53±0.62	8.69±0.60	3.53±0.33	5.63±0.38
Threads per spider	6.5±0.9	11.8±1.8	6.5±0.6	6.0±1.1	7.0±1.0
Relative Young's modulus					
2×	0.35±0.06	0.31±0.02	0.24±0.02	0.58±0.05	0.39±0.03
3×	0.47±0.13	0.46±0.03	0.32±0.02	0.78±0.03	0.50±0.05

Values are means ±1 s.e.m. Unstretched threads had RYM values of 0.083843 (Fig. 5).

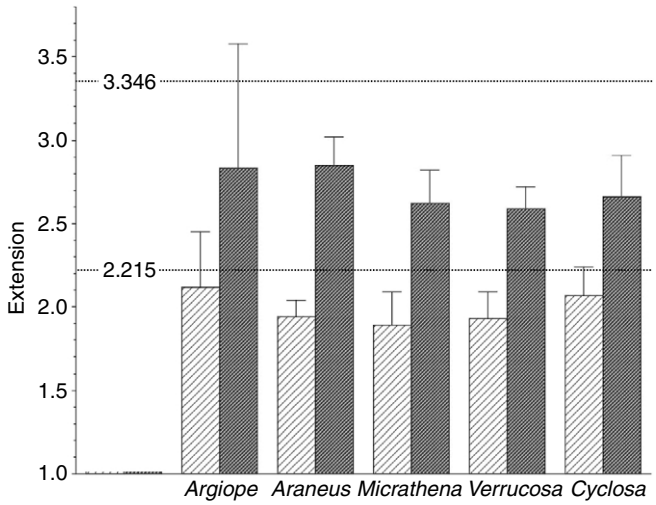

Fig. 3. Achieved thread extension for the five species compared to the intended 2.215 and 3.346× extensions. Light shaded bars represent 2× extensions, and dark shaded bars represent 3× extensions.

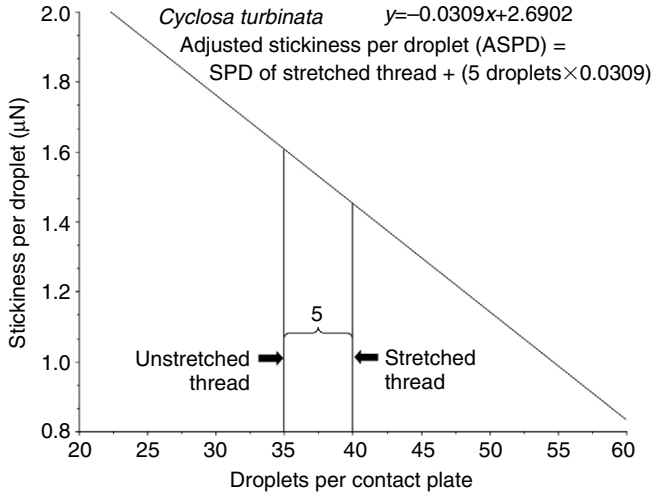

Fig. 4. Relationship between the number of *C. turbinata* thread droplets contributing to thread stickiness, as measured with contact plates of four widths, and the mean stickiness per thread droplet. This example shows how we compensated for a decrease in the per droplet stickiness due to inadequate thread elongation, which resulted in five additional droplets contributing to a thread's stickiness. Multiplying these five droplets by the slope of the regression line and adding this product to the measured stickiness per droplet corrects for the effects of thread elongation, which was less than intended.

we divided this difference by the mean droplet volume of the individual's three thread strands at the three elongations and multiplied this value by 100 to obtain an index that we term the range of intraindividual droplet volume (Table 1).

Evaluating realized thread elongation

Deviations from the intended 2× and 3× thread elongation would compromise our experimental design. Therefore, we evaluated the thread elongation that we achieved by first computing the number of droplets per millimeter thread length (DPMM) from images of each individual's threads at their native lengths and at each of the two elongations. We then divided the DPMM of an individual's unstretched threads by the DPMM of its 2× and 3× stretched thread to determine the elongation that was achieved. As Fig. 3 shows, we achieved less elongation than intended. Our attempts to secure threads to the bars on the caliper's jaws by using a pliable adhesive tape followed by the addition of fast-drying paint may not have prevented the axial fibers of these threads from being pulled through these attachment media. Alternatively, threads were initially elongated as intended but slipped through the adhesive of the double-sided Scotch® tape as they were transferred to the supporting bars of the microscope slide samplers. Although we did achieve progressive thread elongation for all species (Fig. 3), our failure to fully elongate threads resulted in more droplets contacting plates used to measure stretched threads than those used to measure unstretched threads. To correct this problem, we computed stickiness per thread droplet, as explained more fully in the following section.

Computing adjusted stickiness per droplet

We first divide the stickiness registered by contact plates of each width by the number of droplets contacting the plate. Droplet number was computed by multiplying the DPMM for 1×, 2× and 3× elongated threads by the width of the 0.963, 2.133 and 3.222 mm-wide contact plates, respectively. Although this mean stickiness per droplet accounted for most of the effects of incomplete thread elongation, a minor additional adjustment was necessary to account fully for the operation of the SBM. In thread spans of increasing lengths, each additional pair of droplets contributes successively less adhesion, as less adhesion is recruited from interior droplets than from edge droplets (Opell and Hendricks, 2007). Consequently, although increasing the number of droplets in a strand increases the strand's stickiness, it also results in a slight reduction in the mean stickiness per droplet (Fig. 4). Thus, our failure to adequately stretch threads increased the number of droplets that contributed to a strand's stickiness and this, in turn, slightly reduced the stickiness per droplet of 2× and 3× elongated threads. Fig. 4 illustrates this for threads of *C. turbinata*, using previous data (Opell and Hendricks, 2007) to compute the mean stickiness per droplet (SPD) for unstretched threads measured with contact plates of 963, 1230, 1613, and 2133 μm widths. It shows that, as the number of droplets contacting plates of greater widths increases, the thread span's mean SPD decreases.

Consequently, it was necessary to correct the SPD values of under-stretched threads. The relationship between droplet number and SPD described above and illustrated in Fig. 4 provides a mechanism for doing so. By knowing how many additional droplets contacted the plates used to measure the stickiness of 2× and 3× stretched threads than the plate used to measure unstretched thread, it was possible to restore the SPD lost to increases in the number of contacting droplets. In the example of *C. turbinata* (Fig. 4), insufficient thread elongation resulted in five additional droplets contributing to the stickiness of the stretched thread. Multiplying these five additional droplets by the slope of the regression line and adding this product to the measured mean SPD for the stretched thread yields a value that we term adjusted SPD (ASPD), which corrects for the slight reduction in SPD due to the increased number of droplets. We generated similar regressions for *A. marmoreus* from data used in Opell and Hendricks (Opell and Hendricks, 2007) and for *A. aurantia*, *M. gracilis* and *V. arenata* from data that were gathered for a broader survey (B.D.O. and M.L.H., unpublished observations). The regressions for these additional species are: $y=0.0002x+5.1774$, $y=0.0003x+12.4666$, $y=0.0006x+1.8627$, and $y=0.0011x+11.7829$, respectively, where y is the value added to the

measured SPD, and x is the number of additional droplets contacting a plate used to measure the stickiness of stretched threads.

Measuring the breaking length of threads

As the native extensibility of viscous threads differs among species (Opell and Bond, 2001), we judged that our thread elongation procedure probably did not affect the extensibility of each species' axial fibers in the same way. To evaluate this, we measured the breaking lengths of capture threads relative to their native lengths, using the same caliper apparatus described above, the same methods for affixing threads to the bars on this caliper's jaws, and the same rate of elongation to measure the breaking lengths of capture threads. We collected a series of 3 mm-long thread spans from each web, extended these threads and recorded the breaking length of each strand. We then computed breaking factor by dividing a thread's initial length by its length at rupture.

Evaluating breaking factors of threads

Differences in the breaking factors of the five species' threads (Table 1) indicate that our elongations did affect their threads differently. When a viscous capture thread is strained (elongated), its stress initially increases gradually and then in a more pronounced manner as it enters the stress hardened phase of its stress–strain curve prior to rupture (Köhler and Vollrath, 1995; Blackledge and Hayshi, 2006). Thus, at elongations of 3× stretched, the threads of *V. arenata* were much nearer their rupture values and were much stiffer than the 3× stretched threads of the other species. By contrast, at an elongation of 3×, the threads of *M. gracilis* were still quite extensible. Because the analysis of our controlled thread elongations indicated that some thread slippage occurred during the stretching procedure, the breaking factors that we report may be inflated. However, if most of this slippage occurred when stretched threads were transferred from the caliper to the microscope slide samplers, then these breaking factors are not greatly inflated. Whichever scenario is correct, we believe that breaking factors are useful in assessing differences in the residual extensibility of viscous threads in the five species' orb-webs.

The standard index of a fiber's extensibility is its Young's modulus, with higher values indicating stiffer fibers. Young's modulus is computed by dividing stress in MPa by strain, expressed as a percentage of a fiber's initial length. Thus, a fiber's Young's modulus can be computed at any elongation from its stress–strain curve. Although we were not equipped to generate stress–strain curves for threads of the species we studied, we were able to compute an index that we term 'relative Young's modulus' (RYM) for each species' threads at each of their realized elongations. We based these values on the stress–strain curve for the viscous capture threads of *Araneus diadematus* (Köhler and Vollrath, 1995). From this curve, we determined the Young's Modulus at the full range of thread stresses up to and including the thread's rupture value. We then plotted these values as RYM, where Young's modulus at rupture=1, against relative thread elongation, where elongation at rupture=1, and mathematically described this relationship (Fig. 5). For each elongation of each individual's threads we computed a relative thread elongation ratio by dividing the achieved thread elongation by the mean breaking elongation of its species. We then used the regression formula shown in Fig. 5 to assign RYM values to these achieved thread elongations (Table 1, Fig. 6). Although RYM is more appropriate than thread elongation for describing the amount of residual extensibility in a thread's axial fibers, it is based on the thread of a species not included in this study and, therefore, it only approximates residual thread extensibility. The regression model

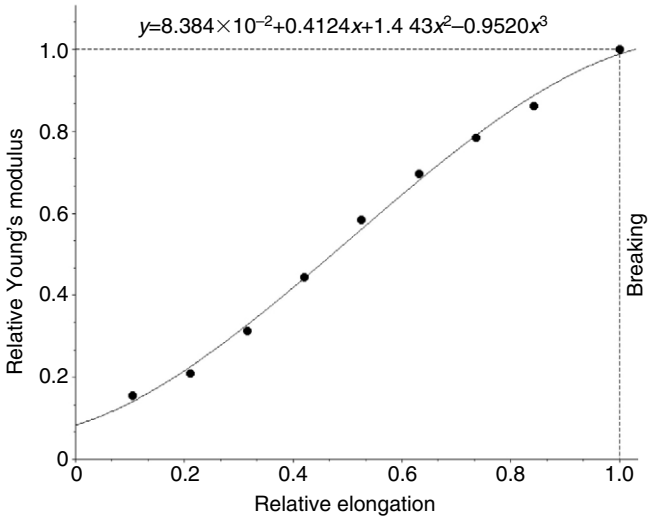

Fig. 5. Plot of relative thread elongation (elongation/elongation at rupture) and relative Young's modulus (Young's modulus/Young's modulus at rupture) derived from the stress–strain curve of *Araneus diadematus* (Köhler and Vollrath, 1995).

assigned a RYM value of 0.083843 to unstretched threads. Although this base value might be regarded as an artifact of the modeling process, it is probably a reasonable estimate because threads were already under some tension in the orb-web and because threads were slightly elongated as their stickiness was being measured.

Testing the effects of droplet volume and thread elongation on stickiness

For each individual's threads at each elongation we determined DV, ASPD and RYM. Within a species, droplet volume is directly related to the stickiness of viscous threads (Opell, 2002; Opell and Schwend, 2007), although this relationship may not be as strong among species (Opell and Schwend, 2008). Moreover, our hypothesis predicted that RYM should contribute negatively to stickiness, as larger values of RYM indicate stiffer threads. We used the SAS statistical package (SAS Inc., Cary, NC, USA) to test the normality of droplet volumes, to compare the droplet volumes of threads stretched to different lengths and to generate regression models that tested the hypothesized contribution of DV and RYM to ASPD in each of the five species. Data were considered normally distributed if $P>0.05$ for a Shapiro–Wilk W-statistic test. We examined normally distributed data with one-way analyses of variance (ANOVA) and *t*-tests (T). Data that were not normally distributed were compared with Kruskal–Wallis χ^2 tests (KW). We considered regression models with $0.10\geqslant P>0.05$ to provide weak support for the hypothesis and $P\leqslant0.05$ to provide strong support for the hypothesis.

Thread elongation clearly altered the RYM of an individual's thread samples (Fig.6). Moreover, the range of intraindividual droplet volume of the 1×, 2× and 3× threads was considerable, from 31 to 61%, and averaged 51% of mean individual droplet volume (Table 1). Given these differences, the separate measurements of the RYM, DV and ASPD that we obtained for each individual's 1×, 2× and 3× threads were largely independent of one another. However, there is still the possibility of a spider-specific effect among the three factors (RYM, DV, individual) that contributed to ASPD. Therefore, we report two sets of P values for each species' regression model: P (EDF1), whose F value was computed using an error degree of

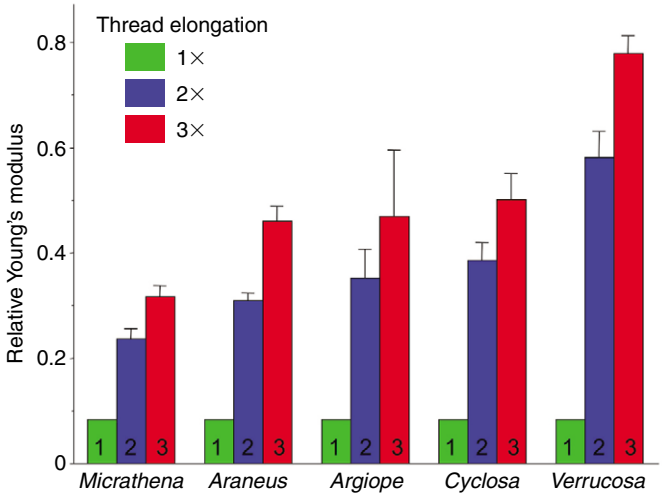

Fig. 6. Relative Young's modulus values for unstretched and stretched threads derived from the curve shown in Fig. 5.

freedom (EDF) based on the number of individuals sampled, and *P* (EDF2), whose EDF was based on a sample size reduced by one-third to account for any effect of measuring the threads of individuals at three elongations. Thus, EDF2 provides a more conservative test of the hypothesis by diminishing the individual component through reduced *F* values and increased *P* values.

RESULTS

Testing hypotheses

Tables 1 and 2 report the thread features and stickiness values for native and elongated threads of the five species. If thread elongation resulted in more viscous material being withdrawn from droplets and distributed along interdroplet regions, then a species' droplet volume should decrease as threads are elongated. In fact, it appears as though there might be a tendency for droplet volume to increase as threads are elongated (Table 1). However, this is not supported by comparisons of either the droplet volumes of threads at their three elongations or of the droplet volumes of the unstretched and 3× threads. For *A. aurantia*, *A. marmoreus*, *M. gracilis*, *V. arenata* and *C. turbinata*, the results of these tests were: KW P=0.3897, KW P=0.2482; ANOVA P=0.2441, T P=0.0944; KW P=0.8208, KW P=0.6272; KW P=0.6977, KW P=0.3258; ANOVA P=0.8749, T P=0.9397, respectively.

In *M. gracilis*, *V. arenata* and *C. turbinata*, DV and RYM jointly explained ASPD in models judged on both full and reduced EDF values (Table 3). In these three species, DV was a significant and positive contributor to ASPD under both full and reduced EDF values. In all species but *A. marmoreus*, RYM was a significant and negative contributor to ASPD under full EDF values. That is, as a thread's extensibility was reduced, its per droplet stickiness also decreased. When EDF2 values were considered, strong support for a negative contribution of RYM remained in *M. gracilis* and *V. arenata* but there was only weak support for a negative contribution of RYM in *A. aurantia* and *C. turbinata*.

Our failure to find a strong support for models of ASPD based on DV and RYM in *A. aurantia* and *A. marmoreus* may result from high DV variance in these species or to a low correlation between the DV and ASPD in the individuals that we studied. The relationships between DV and ASPD for the unstretched threads of *A. aurantia* and *A. marmoreus* were not significant (P=0.1327 and 0.1859, respectively) whereas this relationship was significant for *M. gracilis*, *V. arenata* and *C. turbinata* (P=0.0038, P=0.0061 and 0.0303, respectively).

We used the significant regression models for *M. gracilis*, *V. arenata* and *C. turbinata* to illustrate graphically the contributions of RYM and DV to ASPD (Fig. 7). These models showed that, as threads are elongated, the adhesion attributed to droplet volume alone increasingly exceeded measured ASPD whereas increasing amounts of potential adhesion are lost to reduced thread extensibility.

Axial fibers contribute indirectly to thread stickiness by recruiting the adhesion of multiple droplets. To assess this contribution we used the regression models of *M. gracilis*, *V. arenata* and *C. turbinata* to estimate the percentage of an unstretchced thread's stickiness that can be attributed to the extensibility of its axial fibers. We express this contribution as percent elastic component (PEC), the reduced stickiness of a 3× elongated thread attributed to its lost extensibility

Table 2. Thread stickiness and the environmental conditions under which measurements were taken

	A. aurantia (*N*=4)	*A. marmoreus* (*N*=8)	*M. gracilis* (*N*=9)	*V. arenata* (*N*=10)	*C. turbinata* (*N*=8)
Conditions					
Temperature (°C)	23.8±0.3	24.5±0.2	23.5±0.2	23.9±0.2	24.3±0.03
Relative humidity (%)	42.6±4	44.9±2	46.7±1	46.9±1	44.0±3.3
Barometric pressure (kPa)	134.922±0.400	134.789±0.133	135.189±0.133	135.456±0.133	135.722±0.133
Stickiness (μN)					
Unstretched	101.50±31.74	48.40±4.08	57.76±4.05	149.42±14.22	40.04±2.28
2×	96.44±27.07	65.52±8.70	59.14±4.77	142.42±11.64	42.18±1.98
3×	80.88±4.81	67.85±7.69	45.92±5.96	146.38±15.85	38.48±1.66
Stickiness per droplet (SPD) (μN)					
Unstretched	28.42±5.13	14.80±2.08	6.06±1.16	17.31±2.66	1.86±0.23
2×	25.10±3.36	17.17±2.98	4.51±0.35	14.39±2.75	1.76±0.17
3×	19.18±1.60	18.57±4.32	3.55±0.70	12.73±2.13	1.33±0.08
SPD adjusted for achieved stretch (ASPD) (μN)					
Unstretched	28.42±5.13	14.80±2.08	6.06±1.16	17.31±2.66	1.86±0.23
2×	24.85±3.36	17.56±2.98	4.89±0.44	16.20±2.60	1.80±0.17
3×	20.36±3.84	19.11±4.21	4.05±0.71	15.43±2.08	1.51±0.12

Values are means ±1 s.e.m.

divided by the stickiness of an unstretched thread. The PECs for *M. gracilis*, *V. arenata* and *C. turbinata* threads were 50.0%, 29.2% and 22.5%, respectively, yielding a mean PEC of 33.9%.

Assessing the effects of stress relaxation

When a polymer is elongated and maintained in this strained condition, the resulting stress can cause the fiber to lengthen, thereby reducing this stress. This behavior is known as stress relaxation and was demonstrated (Denny, 1976) to occur in the viscous threads of *Araneus sericatus*. When these threads were strained to 262% of their initial length (87% of their breaking elongations), they registered a stress of $1^{8.65}\,N\,m^{-2}$. Within 10 min, this stress diminished to $1^{8.37}\,N\,m^{-2}$ (52% of their initial stress) and after 38 min they achieved stress equilibrium at a value that was only slightly less [fig. 11 in Denny (Denny, 1976)]. When interpreted in light of the stress–strain curve of this species' viscous threads [fig. 9 in Denny (Denny, 1976)], this shows that, after undergoing stress relaxation, the effective strain of these threads was 227% rather than the initial 262% that they experienced. Thus, if the stress–strain curve of the stress-relaxed thread was unaltered, it appears that stress relaxation restored 13% of the thread's residual elongation and reduced the thread's Young's modulus. The Young's modulus of threads at rupture was 0.367, and at an elongation of 262% it was 0.179. If the stress–strain curve of the stress-relaxed thread was unaltered, the Young's modulus would be 0.115. These values translate into RYM values of 1.00, 0.49 and 0.31, respectively. However, the stress–strain curves of stress-relaxed threads almost certainly have steeper slopes than those of native threads.

The time required to screen and photograph threads before measuring their stickiness allowed all of the threads used in this study to reach their stress relaxation equilibriums. This means that the residual extensibility of all of the stretched threads was probably greater than our indices of relative Young's modulus indicate and was probably proportionately greater for threads that were stretched to a higher percentage of their breaking elongations. The mean realized 3× extensions of the threads of *M. gracilis*, *A. marmoreus*, *A. trifasciata*, *C. turbinata* and *V. arenata*, expressed as a percentage of their mean breaking extensions, were 30%, 43%, 47%, 47% and 75%, respectively. Thus, stress relaxation should have had the most pronounced effect on stretched threads of *V. arenata*.

To assess this effect, we performed an additional regression for *V. arenata* threads using reduced RYM values computed from the data on *A. sericatus*. Relative to breaking elongation, the 3× elongation of *V. arenata* threads was 86% that of *A. sericatus*. As the stress-relaxed RYM of *A. sericatus* threads was 37% less than their elongated RYM, this translates to a 32% reduction in the RYM values of 3× *V. arenata* threads. The mean realized 2× extension of *V. arenata* threads was 53% of their mean breaking extensions. If the RYM of a stress-relaxed thread decreases in proportion to its elongation, then the values of a 2× thread should be 71% that of a 3× thread or 23% that of thread that has not undergone stress relaxation. The regression model based on these modified RYM values is significant (Model *P* EDF1=0.0001, DV *P* EDF1=0.0001, RYM DV *P* EDF1=0.0125) and shows that ASPD is directly related to DV and inversely related to RYM (ASPD=0.001DV–8.923RYM+13.529).

Table 3. Results of regression analyses of the relationship between droplet volume (DV) and relative Young's Modulus (RYM) and adjusted stickiness per droplet (ASPD) that accounts for realized thread elongations

	A. aurantia	*A. marmoreus*	*M. gracilis*	*V. arenata*	*C. turbinata*
Model					
R^2	0.457	0.107	0.637	0.735	0.469
P (EDF1)	0.0640 (9)	0.3064 (21)	0.0001 (24)	0.0001 (27)	0.0013 (21)
P (EDF2)	0.151 (6)	0.455 (14)	0.0001(16)	0.0001 (18)	0.012 (14)
ASPD=DV ×	8.676×10^{-5}	1.676×10^{-5}	3.530×10^{-4}	9.877×10^{-4}	1.550×10^{-3}
+ RYM ×	–22.750	16.654	–10.008	–6.697	–0.874
+ (intercept)	25.857	11.481	4.642	13.507	1.423
DV					
P (EDF1)	0.2601 (9)	0.5527 (21)	0.0001 (24)	0.0001 (27)	0.0013 (21)
P (EDF2)	0.352 (6)	0.650 (14)	0.0001 (16)	0.0001 (18)	0.009 (14)
RYM					
P (EDF1)	0.0352 (9)	0.1583 (21)	0.0016 (24)	0.0094 (27)	0.0385 (21)
P (EDF2)	0.090 (6)	0.250 (14)	0.011(16)	0.035 (18)	0.092 (14)

Two *P* values are given, *P* (EDF1), whose error degree of freedom was based on the number of individuals sampled, and *P* (EDF2), whose error degree of freedom was two-thirds of this value. The numbers in parentheses following *P* values are the sample size on which these *P* values are based.

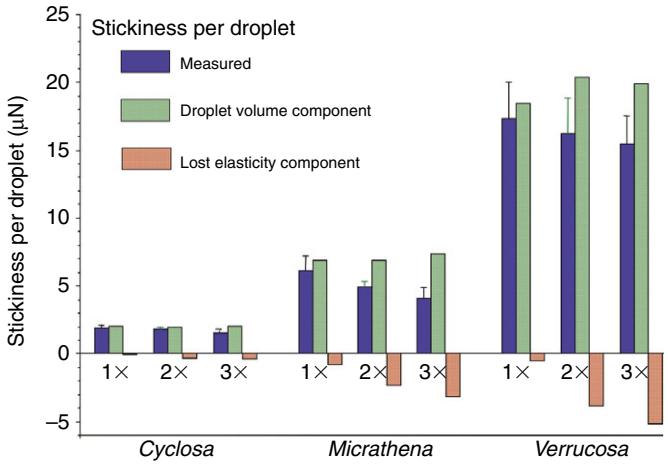

Fig. 7. Adhesive components of the threads of *M. gracilis*, *V. arenata* and *C. turbinata* based on regression models (Table 3) of the positive contributions of droplet volume and the negative contribution of relative Young's modulus to mean stickiness per thread droplet.

DISCUSSION

Our results support the hypothesized positive contribution of a viscous thread's axial fiber extensibility to its stickiness. When threads are stretched and their extensibility is reduced, their per droplet stickiness decreases. We observed this response both in threads of *M. gracilis*, which had the greatest native extensibility, and in threads of *V. arenata*, which had the least. We also observed it in threads whose droplet volumes differed by a factor as great as 152 and whose droplet spacing differed by a factor as great as 6. These findings are consistent with the operation of a SBM that enhances the stickiness of viscous capture threads by recruiting the adhesion of droplets interior to the edges of a thread's contact with a surface (Opell and Hendricks, 2007).

Our attempt to evaluate the effect of stress relaxation on stretched threads used the conservative assumption that the slope of the stress–strain curve of stress-relaxed threads is identical to that of threads that have not undergone stress relaxation. Nonetheless, it confirmed that thread extensibility contributes positively to the stickiness of *V. arenata* threads, which were elongated to a much greater percentage of their breaking lengths than were threads of the other species. Consequently, we believe that stress relaxation did not confound the broader conclusions of our study. A complete explanation of viscous thread performance must incorporate this phenomenon, although the preliminary calculations that we present suggest that this will be challenging.

The molecular structure of silk affects its mechanical properties (Hayashi et al., 1999; Hayashi et al., 2001; Hayashi et al., 2004; Hayashi and Lewis, 2001; Craig, 2003; Ayoub et al., 2007) and appears to explain intraspecific (Blackledge and Hayashi, 2006) and interspecific (Swanson et al., 2006a; Swanson et al., 2006b) differences in thread properties. However, the observed 2.5-fold difference among the breaking factors of the five species' viscous threads (Table 1) cannot be attributed solely to differences in the molecular composition of their axial fibers. As we measured threads at their native, in-web tensions and did not standardize their tensions prior to measuring their breaking factors, we were unable to factor out the contribution that differences in web construction behavior may have made to the observed differences in thread breaking factors. Members of some species may stretch their capture threads more than others before they attach them to the web's radial lines. If they do, then a greater portion of the potential extensibility of these threads would have been expended, leaving them with less usable extensibility.

The mean 33.9% lost adhesion that can be attributed to reduced extensibility in the 3× stretched threads documents the important contribution that thread extensibility makes to thread stickiness. Threads of all species could be elongated more than the realized 3× extensions on which this estimate was based. However, this 33.9% is probably a reasonable estimate of the typical contribution of axial fiber extensibility to thread adhesion because features of orb-web architecture constrain the elongation that viscous threads undergo when intercepting and retaining prey. Insects usually strike multiple spiral turns, thereby distributing impact forces and struggling stresses over several thread spans. Moreover, aerodynamic dampening helps vertical orb-webs absorb the forces of prey impact as webs flex through the air (Lin et al., 1995). Even this web flexibility is constrained by the combined extensibility of the web's radial and capture lines (Craig, 1987; Craig, 2003).

Intraspecific differences in droplet volume, droplet spacing and maximum thread extensibility made it challenging to evaluate the contribution of axial fiber extensibility to thread adhesion. Only by accounting for each of these variables was it possible to document the role of axial fiber extensibility in thread adhesion. Interspecific differences in maximum thread extensibility and stickiness per droplet volume made it impossible to develop a more general model that describes the performance of the five species' threads. This may indicate that each species' capture threads comprise a unique and highly tuned system whose performance integrates the axial fiber's native extensibility, the extensibility realized after the thread is deposited in a web, the thread's droplet spacing, and the adhesion and plasticity of individual thread droplets.

Caitlin Flora and Genine Lipkey assisted with fieldwork. Harry Schwend helped compute RYM values and provided suggestions for improving figures. National Science Foundation grant IOB-0445137 supported this research.

LIST OF ABBREVIATIONS

ASPD	adjusted stickiness per droplet
DPMM	droplets per millimeter thread length
DV	droplet volume
EDF	error degree of freedom
PEC	percent elastic component
RYM	relative Young's modulus
SBM	suspension bridge mechanism
SPD	stickiness per droplet

REFERENCES

Ayoub, N. A., Garb, J. E., Tinghitella, R. M., Collin, M. A. and Hayashi, C. Y. (2007). Blueprint for a high-performance biomaterial: full-length spider silk genes. *PLoS ONE* **2 e514**, 1-13.

Blackledge, T. A. and Hayashi, C. Y. (2006). Unraveling the mechanical properties of composite silk threads spun by cribellate orbweaving spiders. *J. Exp. Biol.* **209**, 3131-3140.

Chacón, P. and Eberhard, W. G. (1980). Factors affecting numbers and kinds of prey caught in artificial spider webs with considerations of how orb-webs trap prey. *Bull. Br. Arachnol. Soc.* **5**, 29-38.

Coddington, J. A. (1986). The monophyletic origin of the orb-web. In *Spiders: Webs, Behavior and Evolution* (ed W. A. Shear), pp. 319-363. Stanford: Stanford University Press.

Coddington, J. A. (1989). Spinneret silk spigot morphology: evidence for the monophyly of orb-weaving spiders, Cyrtophorinae (Araneidae), and the group Theridiidae plus Nesticidae. *J. Arachnol.* **17**, 71-96.

Craig, C. L. (1987). The ecological and evolutionary interdependence between web architecture and web silk spun by orb web weaving spiders. *Biol. J. Linn. Soc.* **30**, 135-162.

Craig, C. L. (2003). *Spider Webs and Silk: Tracing Evolution from Molecules to Genes to Phenotypes*. New York: Oxford University Press.

Denny, M. (1976). Physical properties of spider silks and their role in design of orb-webs. *J. Exp. Biol.* **65**, 483-506.

Eberhard, W. G. (1986). Effect of orb-web geometry on prey interception and retention. In *Spiders, Webs, Behavior, and Evolution* (ed. W. A. Shear), pp. 70-100. Stanford: Stanford University Press.

Eberhard, W. G. (1988). Combing and sticky silk attachment behaviour by cribellate spiders and its taxonomic implications. *Bull. Br. Arachnol. Soc.* **7**, 247-251.

Eberhard, W. G. (1989). Effects of orb-web orientation and spider size on prey retention. *Bull. Br. Arachnol. Soc.* **8**, 45-48.

Eberhard, W. G. (1990). Function and phylogeny of spider webs. *Annu. Rev. Ecol. Syst.* **21**, 341-372.

Eberhard, W. G. and Pereira, F. (1993). Ultrastructure of cribellate silk of nine species in eight families and possible taxonomic implications. (Araneae: Amaurobiidae, Deinopidae, Desidae, Dictynidae, Filistatidae, Hypochilidae, Stiphidiidae, Tengellidae). *J. Arachnol.* **21**, 161-174.

Foelix, R. F. (1996). *Biology of Spiders*, 2nd edn. New York: Oxford University Press.

Garb, J. E., DiMauro, T., Vo, V. and Hayashi, C. Y. (2006). Silk genes support the single origin of orb-webs. *Science* **312**, 1762.

Griswold, C. E., Coddington, J. A., Hormiga, G. and Scharff, N. (1998). Phylogeny of the orb-web building spiders (Araneae, Orbiculariae: Deinopoidea, Araneoidea). *Zool. J. Linn. Soc.* **123**, 1-99.

Hawthorn, A. C. and Opell, B. D. (2003). van der Waals and hygroscopic forces of adhesion generated by spider capture threads. *J. Exp. Biol.* **206**, 3905-3911.

Hayashi, C. Y. and Lewis, R. V. (2001). Spider flagelliform silk: lessons in protein design, gene structure, and molecular evolution. *BioEssays* **23**, 750-756.

Hayashi, C. Y., Shipley, N. H. and Lewis, R. V. (1999). Hypotheses that correlate the sequence, structure, and mechanical properties of spider silks. *Int. J. Biol. Macromol.* **24**, 271-275.

Hayashi, C. Y., Blackledge, T. A. and Lewis, R. V. (2004). Molecular and mechanical characterization of aciniform silk: uniformity of iterated sequence modules in a novel member of the spider silk fibroin gene family. *Mol. Biol. Evol.* **21**, 1950-1959.

Köhler, T. and Vollrath, F. (1995). Thread biomechanics in the two orb-weaving spiders *Araneus diadematus* (Araneae, Araneidae) and *Uloborus walckenaerius* (Araneae, Uloboridae). *J. Exp. Zool.* **271**, 1-17.

Lin, L. H., Edmonds, D. T. and Vollrath, F. (1995). Structural engineering of an orb-spider's web. *Nature* **373**, 146-148.

Opell, B. D. (1998). Economics of spider orb-webs: the benefits of producing adhesive capture thread and of recycling silk. *Funct. Ecol.* **12**, 613-624.

Opell, B. D. (1999). Changes in spinning anatomy and thread stickiness associated with the origin of orb-weaving spiders. *Biol. J. Linn. Soc.* **68**, 593-612.

Opell, B. D. (2001). Cribellum and calamistrum ontogeny in the spider family Uloboridae: linking functionally related but separate silk spinning features. *J. Arachnol.* **29**, 220-226.

Opell, B. D. (2002.). Estimating the stickiness of individual adhesive capture threads in spider orb-webs. *J. Arachnol.* **30**, 494-502.

Opell, B. D. and Bond, J. E. (2001). Changes in the mechanical properties of capture threads and the evolution of modern orb-weaving spiders. *Evol. Ecol. Res.* **3**, 567-581.

Opell, B. D. and Hendricks, M. L. (2007). Adhesive recruitment by the viscous capture threads of araneoid orb-weaving spiders of araneoid orb-weaving spiders. *J. Exp. Biol.* **210**, 553-560.

Opell, B. D. and Schwend, H. S. (2007). The effect of insect surface features on the adhesion of viscous capture threads spun by orb-weaving spiders. *J. Exp. Biol.* **210**, 2352-2360.

Opell, B. D. and Schwend, H. S. (2008). Persistent stickiness of viscous capture threads produced by araneoid orb-weaving spiders. *J. Exp. Zool.* **309A**, 11-16.

Opell, B. D. and Schwend, H. S. (in press). Adhesive efficiency of spider prey capture threads. *Zoology*.
Peters, H. M. (1984). The spinning apparatus of Uloboridae in relation to the structure and construction of capture threads (Arachnida, Araneida). *Zoomorphology* **104**, 96-104.
Peters, H. M. (1986). Fine structure and function of capture threads. In *Ecophysiology of Spiders* (ed W. Nentwig), pp. 187-202. New York: Springer Verlag.
Peters, H. M. (1992). On the spinning apparatus and structure of the capture threads of *Deinopis subrufus* (Araneae, Deinopidae). *Zoomorphology* **112**, 27-37.
Peters, H. M. (1995). Ultrastructure of orb spiders' gluey capture threads. *Naturwissenschaften* **82**, 380-382.
Platnick, N. I. (2008). *The World Spider Catalog*, v. 8.5. http://research.amnh.org/entomology/spiders/catalog/INTRO1.html.
Swanson, B. O., Blackledge, T. A., Beltrán, J. and Hayashi, C. Y. (2006a). Variation in the material properties of spider dragline silk across species. *Appl. Physics A* **82**, 213-218.
Swanson, B. O., Blackledge, T. A., Summers, A. P. and Hayashi, C. Y. (2006b). Spider dragline silk: correlated and mosaic evolution in high-performance biological materials. *Evolution* **60**, 2539-2551.
Tillinghast, E. K., Townley, M. A., Wight, T. N., Uhlenbruck, G. and Janssen, E. (1993). The adhesive glycoprotein of the orb-web of *Argiope aurantia* (Araneae, Araneidae). *Mat. Res. Soc. Symp. Proc.* **292**, 9-23.
Townley, M. A. (1990). Compounds in the droplets of the orb spider's viscid spiral. *Nature* **345**, 526-528.
Townley, M. A., Bernstein, D. T., Gallanger, K. S. and Tillinghast, E. K. (1991). Comparative study of orb-web hydroscopicity and adhesive spiral composition in three areneid spiders. *J. Exp. Zool.* **259**, 154-165.
Vollrath, F., Fairbrother, W. J., Williams, R. J. P., Tillinghast, E. K., Bernstein, D. T., Gallagher, K. S. and Townley, M. A. (1990). Compounds in the droplets of the orb spider's viscid spiral. *Nature* **345**, 526-528.
Vollrath, F. and Tillinghast, E. K. (1991). Glycoprotein glue beneath a spider web's aqueous coat. *Naturwissenschaften* **78**, 557-559.